Construction and Building Materials 220 (2019) 149–160

Contents lists available at ScienceDirect

Construction and Building Materials

journal homepage: www.elsevier.com/locate/conbuildmat

Self-stress sensing smart concrete containing fine steel slag aggregates and steel fibers under high compressive stress

Seon Yeol Lee [a], Huy Viet Le [a,b], Dong Joo Kim [a,*]

[a] Department of Civil and Environmental Engineering, Sejong University, 98 Gunja-dong, Gwangjin-gu, Seoul 143-747, South Korea
[b] Department of Civil Engineering, Hanoi University of Mining and Geology, Hanoi, Viet Nam

HIGHLIGHTS

- MSF containing FSSAs and steel fibers produced great piezoelectric response.
- The electrical resistivity reduction of MSF was clearly higher than that of other smart concretes.
- Smart anchorage using MSF was applied to prestressing steel anchorage zone to monitor the loss of prestressing stress.
- An equation correlating stress and electrical resistivity of smart anchorage was obtained.

ARTICLE INFO

Article history:
Received 25 March 2019
Received in revised form 27 May 2019
Accepted 31 May 2019
Available online 8 June 2019

Keywords:
Electrical resistivity
Self-sensing
Fine steel slag aggregate (FSSA)
Steel fiber
Smart concrete anchorage

ABSTRACT

This study investigated the piezoelectric response of a smart concrete (MSF) containing fine steel slag aggregates (FSSAs) and steel fibers under high compression by measuring the alternative current impedance. The electrical resistivity of MSF notably decreased (15.65%) with the increase in the applied compressive stress from 20 to 100 MPa, whereas the electrical resistivities of smart concretes containing only FSSAs or steel fibers or both multiwalled carbon nanotubes and steel fibers reduced by 9.62, 12.37, and 9.30%, respectively. The MSF with a linear piezoelectric response under compression (until 60 MPa) was applied to a prestressing steel anchorage zone to monitor the loss of prestressing stress.

1. Introduction

Smart concretes with a self-sensing ability have great potential in the field of structural health monitoring (SHM) for infrastructures. They can significantly enhance the durability and safety of infrastructures such as high-rise buildings, large span bridges, dams, tunnels, offshore structures, and nuclear power plants [1]. Furthermore, smart concrete can be applied to prestressing steel (PS) anchorage zone, requiring a high compressive strength as well as crack resistance, to monitor the loss of prestressing stress [2]. The level of prestressing stress can be monitored based on the electromechanical response of the smart concrete in the PS anchorage zone [2].

Commercial sensors used for SHM include electric strain gauges, piezo ceramic transducers, fiber Bragg grating sensors, fiber optical sensors, and lead zirconate titanate sensors [3–6]. Moreover, to monitor the loss of prestressing stress, elastomagnetic sensors [7], fiber optic sensors [8], and long-gauge fiber Bragg grating sensors [9] have been applied. However, most commercial sensors have low durability and consequently require periodic repair and maintenance.

To overcome the drawbacks of current sensors, several smart concretes containing electrically conductive functional fillers, including carbon nanotubes (CNTs), multi-wall carbon nanotubes (MWCNTs), graphene, graphite nanofibers, nickel, carbon black (CB), steel fibers, carbon nanofibers (CNF), and carbon fibers (CFs) have been developed [10–28]. The addition of conductive fillers enhances the conductive network within the composites and helps

Abbreviations: AC, alternative current; DC, direct current; FCR, fractional change in resistivity; FSSA, fine steel slag aggregate; MF, smart concrete containing steel fiber; MFMW, smart concrete containing MWCNTs and steel fibers; MS, smart concrete containing FSSAs; MSF, smart concrete containing both steel fibers and FSSAs; MWCNT, multi-wall carbon nanotube; PS, prestressing steel; UHPC, ultra-high performance concrete.

* Corresponding author.
E-mail address: djkim75@sejong.ac.kr (D.J. Kim).

https://doi.org/10.1016/j.conbuildmat.2019.05.197
0950-0618/

improve the self-sensing capacity; however, the self-stress sensing capacity of smart concretes is limited (within 20 MPa) under compression owing to the nonlinear correlation between the applied stress and the electrical resistivity, as listed in Table 1.

Fig. 1 shows the typical electromechanical response of a smart concrete under compression, divided into three stages: a linearly decreasing phase, a stable phase, and an increasing phase [1]. The three stages correspond to pressure compaction, generation of micro cracks, and crack propagation, respectively [1]. The compacting pressure brings the functional fillers closer, thus improving the conductive network inside the composite; the generation of microcracks results in the destruction and reconstruction of the conductive network inside the composite; and the propagation of cracks leads to the breakdown of the conductive network. Thus, to apply to the PS anchorage zone, a smart concrete with the linear piezoelectric response under high compression can be developed by enhancing compressive strength of the concrete in elastic region (no crack generation) and structured conductive network of fillers. You et al. [29] recently reported that the addition of the CNT improved the self-sensing ability of the ultra-high performance concrete (UHPC) that was activated by the formation of cracks and greater amount of CNT produced a greater the self-sensing ability. However, there was a minor fractional change in the electrical resistivity of the UHPC containing both CNTs and steel fibers under compression within elastic region prior to matrix cracking point, which might have been due to the highly densified microstructure and/or non-uniform distribution of the CNTs in the UHPC matrix at very low water-to-cement ratios [29].

In this study, the self-stress sensing ability of the UHPC within elastic region prior to matrix cracking could be successfully developed by adding fine steel slag aggregates (FSSAs) and steel fibers. Fine steel slag aggregates with maximum diameter of 0.39 mm were applied (instead of silica sand) to the matrix of the smart concrete to enhance its electrical conductivity based on quantum tunneling effects whereas short steel fibers with 6 mm in length were reinforced the UHPC to prevent any micro-cracking within the linear elastic region and to improve the electrically conductive network as well. The steel slag aggregates would be easier to be uniformly distributed in the UHPC matrix and consequently enhance the overall electrical conductivity. Han et al. [1] also reported that steel slag was one of potential conductive fillers for enhancing the conductive network within the matrix. In addition, steel slags improved the workability and mechanical properties of concrete [30,31]. However, the incorporation of steel slags as aggregate in concrete might result in a potential volumetric instability associated with the hydration of free CaO and/or MgO in the slags [32]. Lu et al. [33] reported that use of basic oxygen furnace (BOF) slag fines in ordinary Portland cement significantly reduced the compressive strength and slightly increased the volume expansion of the mortars.

However, researchers recently indicated that adequate aging/weathering and treatments can enhance the hydrolyses of free CaO and MgO to mitigate the instability of concrete with steel slags [32]. Rondi et al. [34] reported that the volumetric expansion of fresh concrete mixtures with 100% electric arc furnace (EAF) steel slag as aggregate was lower than the limit value of 0.5% while their compressive strengths showed a stable behavior after a period of one year. The FSSAs used in this research are the electric arc furnace steel slag, produced by ECOMAISTER Company using slag atomizing technology. The chemical properties of FSSAs include SiO_2, Al_2O_3, CaO, MgO, Fe_2O_3, and others with corresponding component ratios of 13.10, 6.31, 24.1, 3.68, 38.3, and 14.01%. Although the company reported that the FSSAs containing very low content of free-CaO (0.1–0.3 wt%) showed in the volumetric stability in long term, the effect of steel slag expansion on the long term structural safety should be further investigated.

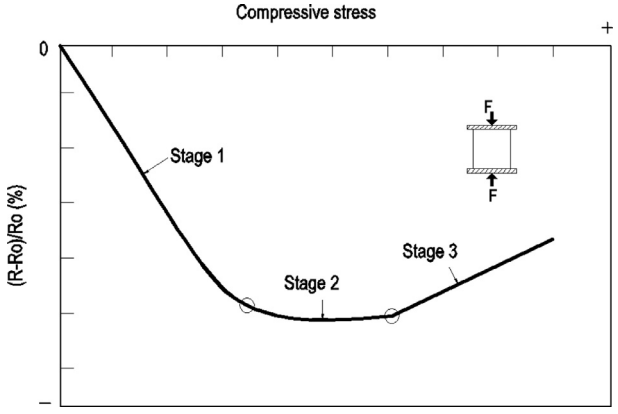

Fig. 1. Typical electromechanical response of smart concrete under compression [1].

The specific objectives of the study are: (1) to investigate the self-stress sensing ability (the electromechanical response) of smart concrete (made from the UHPC containing both FSSAs and steel fibers) under compression in comparison with that of smart concretes made from the UHPCs containing other fillers and (2) to investigate the self-stress sensing capacity of a smart concrete anchorage, made from the UHPC containing both FSSAs and steel fibers, for monitoring the level of prestressing stress.

2. Smart concretes and AC impedance measurement

The self-stress sensing capacity of a smart concrete is based on its piezoelectric response under external load. The change in the electrical resistivity of smart concrete generally originates from the changes in the electrically conductive networks including conductive fillers and pore solution systems [35,36]. The self-sensing ability can be described by the relationship between the fractional change in the electrical resistance and the stress according to Eq. (1).

Table 1
Self-stress sensing capacity of smart concretes.

No	Ref.	Maximum stress sensing (MPa)	*FCR*	Functional filler	W/C	f_c (MPa)
1	Han [10]	6		CNT	0.6	
2	Han [11]	6		CNT	0.4	
3	Han [13]	0.5	0.18	Nickel	0.66	
4	Wen [14]	6.0	0.3	Steel fiber	0.35	
5	Han [19]	20	0.2	CF and CB		40
6	Chung [20]	16	0.3	CF		
7	Monteiro [21]	9.4	0.03	CB	0.5	18
8	Konsta [22]	4	0.05	CNF, CNT	0.3	
9	Han [23]	12		CNT		40

f_c: compressive strength; *FCR*: fractional change in resistance.

$$\frac{\Delta R}{R_o} = \frac{\Delta \rho}{\rho_o} = f(\sigma) \quad (1)$$

where ΔR ($\Delta \rho$) is the absolute change in the electrical resistance (resistivity), R_o (ρ_o) is the initial electrical resistance (resistivity), and $f(\sigma)$ is a function of stress [1].

The change in the electrical resistivity of a smart concrete has been generally measured using alternative current (AC) measurements [37,38] or direct current (DC) measurements [39–42]. The AC measurement is preferred to assess the electrical resistivity of cementitious materials to avoid errors induced by the polarization of the electrodes or variation in the properties over time due to ion migration [37]. The electrical impedance spectroscopy, determined by AC measurement, of cementitious composites are generally represented using a Nyquist plot [43–45]. The Nyquist plot is parameterized in terms of the frequency, which decreases from left (high frequency) to right (low frequency): at low frequencies, the passive layer insulates the fibers whereas it becomes short-circuited at high frequencies, thereby allowing current to flow through the fibers [38]. In the Nyquist plot, i.e., the imaginary impedance ($-Z''$)–real impedance (Z') plot, the electrical impedance spectroscopy of plain cementitious materials are characterized by a single arc, describing the material behavior (material arc), whereas a two-arc formation represents the response of steel fiber-reinforced cementitious materials [38]. The composite resistance R_{cusp} is determined by a value of the real impedance (Z') at the cusp between the two material arcs and accounts for the combined transfer of the ionic current through the electrolyte and the electron current through the conductive fillers [38]. The electrical resistivity (ρ) of the specimens was calculated from the measured composite resistance (R_{cusp}) using Eq. (2).

$$\rho = R_{cusp}\frac{A}{L} \quad (2)$$

where A is the cross-sectional area, and L is the gauge length between the two electrodes. Moreover, an AC measurement with a fixed frequency can be used to measure the history of the electrical resistivity response of the composite [29].

3. Experimental

An experimental program was designed to investigate the self-stress sensing ability of a smart concrete containing both steel fibers and FSSAs (MSF). Cubic compressive specimens with dimensions of 50 mm × 50 mm × 50 mm were made to compare the self-stress sensing ability of the MSF with those of three other smart concretes: ones containing steel fibers (MF), FSSAs (MS), and MWCNTs and steel fibers (MFMW). The MFMW was prepared to compare the effect of the MWCNTs and FSSAs on the self-stress sensing ability of the UHPC matrices under compression. Fig. 2 shows the images of the short steel fibers, FSSAs, and MWCNTs. Moreover, the cubic specimens were used to investigate the effects of temperature (ranging from 5 to 40 °C) and humidity (ranging from 30 to 100%) on the electrical resistivity of the MSF. On the other hand, a smart concrete anchorage made from the MSF with dimensions of 200 mm × 200 mm × 300 mm was designed for a 7-wire strand (diameter of 15.2 mm; tensile strength of 2160 MPa), as shown in Fig. 3. If the level of prestressing stress is assumed to be 80% of the tensile strength of the 7-wire strand, the compressive stress of the smart concrete anchorage would be approximately 50 MPa. The electrical impedance spectroscopy response of the four smart concretes (MSF, MS, MF, and MFMW) was investigated under controlled compressive stresses of 20, 40, 60, 80, and 100 MPa. An AC measurement (SI 1260 impedance/gain-phase analyzer machine) with varying frequency was used to investigate the electrical impedance spectroscopy response of the cubic compressive specimens under controlled stresses and the electrical resistivity response of the MSF under the temperature and humidity conditions mentioned previously. An AC measurement with a fixed frequency was used to investigate the history of the electromechanical response of the smart concrete anchorage under compression.

3.1. Materials and specimen preparation

Table 2 summarizes the compositions (by weight ratio) of the smart concretes. Table 3 lists the properties of the conductive fillers including those of the steel fibers, FSSAs, and MWCNTs. The diameter and length of the short smooth steel fibers were 0.2 and 6.0 mm, respectively. The FSSAs were ball-shaped with a maximum diameter of 0.39 mm. The diameter of the MWCNTs ranged from 0.05 to 0.2 μm, and their length was approximately 10 μm. The polycarboxylate based super-plasticizer (30% solid and 70% water) reducing or eliminating the attractive interparticles forces that cause yield stresses [46] was used to improve workability of matrices.

A Hobart-type laboratory mixer with a 20-L capacity was used to prepare the smart concrete specimens. In preparing the MF, MS, and MSF mixtures, the components of the matrices (including the silica fume, cement, silica powder, and FSSAs or sand) were first dry-mixed for 5 min. The FSSAs were used instead of sand in the MSF and MS. Water was then added to the mixture, and the mixture was further mixed for 5 min. Super-plasticizers were gradually added and further mixed for approximately 5 min. For both the MSF and MF specimens, as the mixtures showed suitable workability and viscosity for a uniform fiber distribution, the short smooth fibers were carefully dispersed by hand into the mortar mixtures, and the mixtures containing the fibers were then mixed for 1 min.

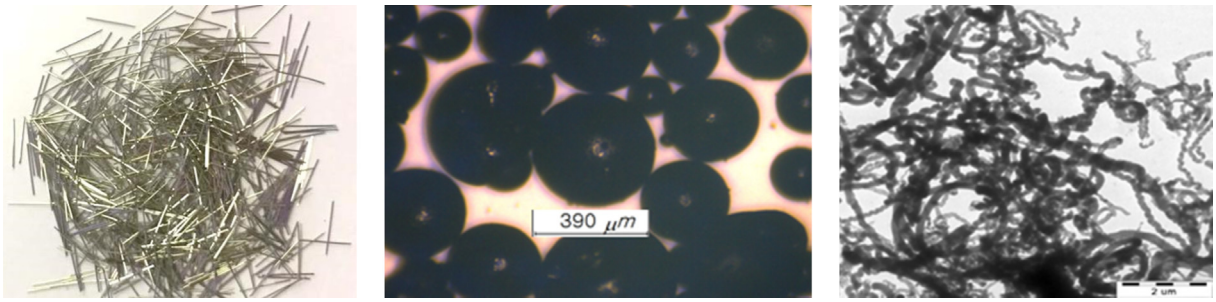

c) Short steel fiber a) Fine steel slag aggregates b) MWCNT

Fig. 2. Images of conductive materials.

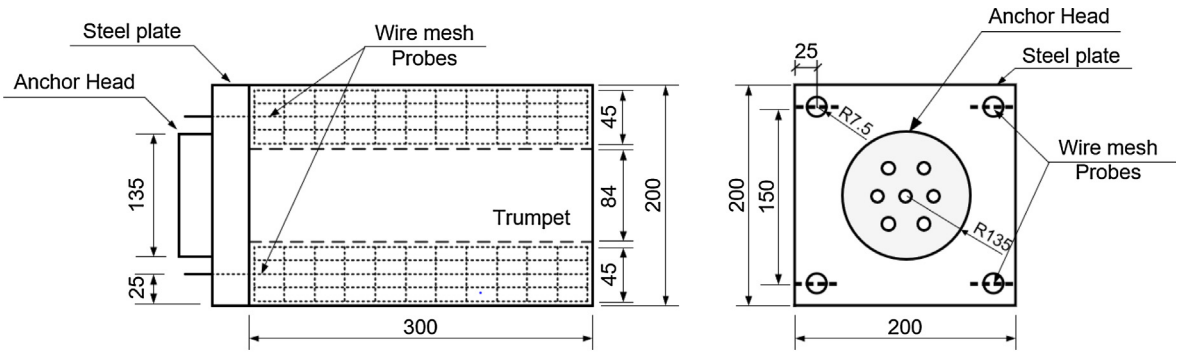

a) A design of the smart concrete anchorage specimens

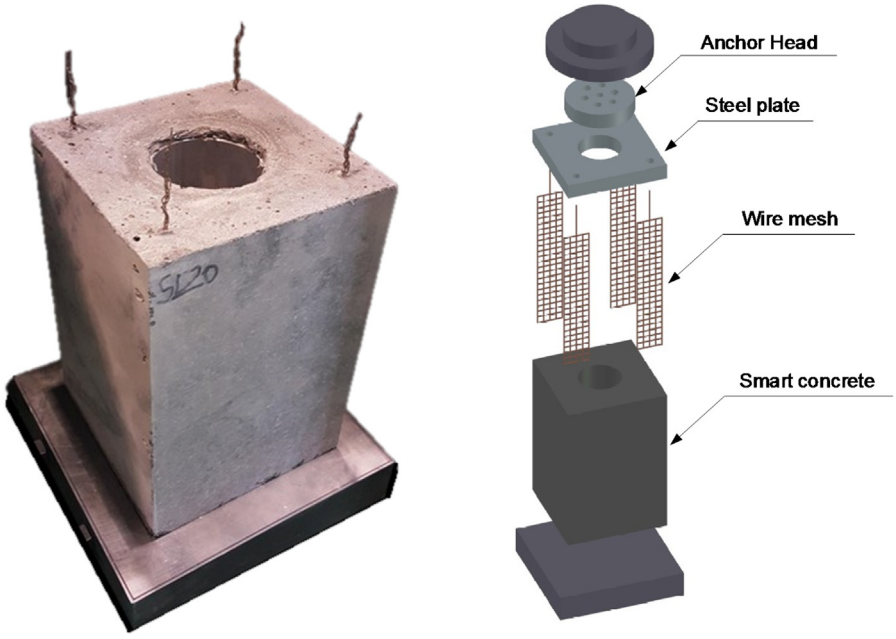

b) A smart concrete anchorage mold c) A smart concrete anchorage specimen

Fig. 3. A smart concrete anchorage specimen using MSF matrix.

Table 2
Composition of matrix by weight ratio.

No.	Cement	Silica fume	Silica powder	Silica sand	Steel slag	Water	SP	MW CNT	Deformer (*)	Fiber (Vol. %)	Flow test (mm)	f_c (MPa)
M	1.0	0.15	0.25	1.0	–	0.2	0.042	–	–	–	245	154 (5)
MF	1.0	0.15	0.25	1.0	–	0.2	0.039	–	–	2.0	268	202 (12)
MS	1.0	0.15	0.25	–	1.0	0.2	0.044	–	–	–	280	180 (8)
MSF	1.0	0.15	0.25	–	1.0	0.2	0.042	–	–	2.0	280	184 (10)
MFMW	1.0	0.15	0.25	1.0	–	0.2	0.098	0.5	0.25	2.0	242	155 (7)

SP: Super plasticizer containing 25% solid and 75% water; MWCNT: Multi-walled carbon nanotube.
* : Weigh percentage of cement; fc: compressive strength. The values in brackets are the standard deviation of the compressive strength.

Table 3
Properties of conductive materials.

Type	Diameter (μm)	Length (mm)	Tensile strength (MPa)	Elastic modulus (GPa)
Steel fiber	200	6.0	2104	200
Steel slag	<390	–	–	–
MWCNT	0.005–0.020	10×10^{-3}	–	–

On the other hand, the MFMW mixture was prepared as follows: (1) A sonicator, operated at an amplitude of 50% and a cycle time of 15 s, was used to distribute the MWCNTs in the solution including water and half the amount of a superplasticizer for 2 h; (2) Silica fume was added to the solution, and further sonication was conducted for 3 to 5 min; (3) Cement, silica sand, and silica powder were dry mixed, added to the solution containing the silica fume, and further mixed for 3 min; (4) The remaining amount of the superplasticizer was added to the mixture; (5) A deformer (Tributyl phosphate from Aladdin Industrial Corporation, USA) was added to the mixture and further mixed for 3 min to eliminate air bubbles in the mixture; and (6) Finally, short steel fibers were added to the mixture and further mixed for 1 min.

The MF, MFMW, and MS mixtures were poured into cubic molds, while the MSF matrix was poured into both the cubic and smart concrete anchorage molds with slight vibration. A smart concrete anchorage was made from MSF, as shown in Fig. 3. A steel cylinder with a diameter of 0.84 mm and a length of 280 mm, instead of a trumpet in pre-stressed concrete, was fixed in the mold using glue, as shown in Fig. 3b. Copper wire meshes (width of 0.45 mm) were embedded in the specimens as electrodes for measuring their electrical resistivity. The distance between the two electrodes was 20 mm for the cubic compressive specimens, whereas it was 150 mm for the smart concrete anchorage specimens.

All the specimens were covered with plastic sheets and stored at room temperature (20 ± 2 °C) for 48 h, after demolding. They were then cured in a water tank at 90 °C for three days. The specimens were dried for 24 h prior to testing. Table 2 lists both the flow and compressive strength values of the smart concretes (without embedded wire meshes).

3.2. Test setup

Fig. 4 shows the experimental setup for determining the electrical resistivity response of the cubic specimens. Fig. 5 shows the setup for the smart concrete anchorage. A universal testing machine (UTM) was used for the compressive tests, whereas the SI 1260 impedance/gain-phase analyzer machine was used to measure the electrical impedance spectroscopy response during the tests. The UTM was under load control to maintain loads of 50, 100, 150, 200, and 250 kN for 200 s, corresponding to compressive stresses of 20, 40, 60, 80, and 100 MPa, respectively. The AC measurement technique (with frequency ranging from 1 Hz to 10 MHz at a voltage of 250 mV and data of 10 points per decade) was used to measure the electrical impedance spectroscopy

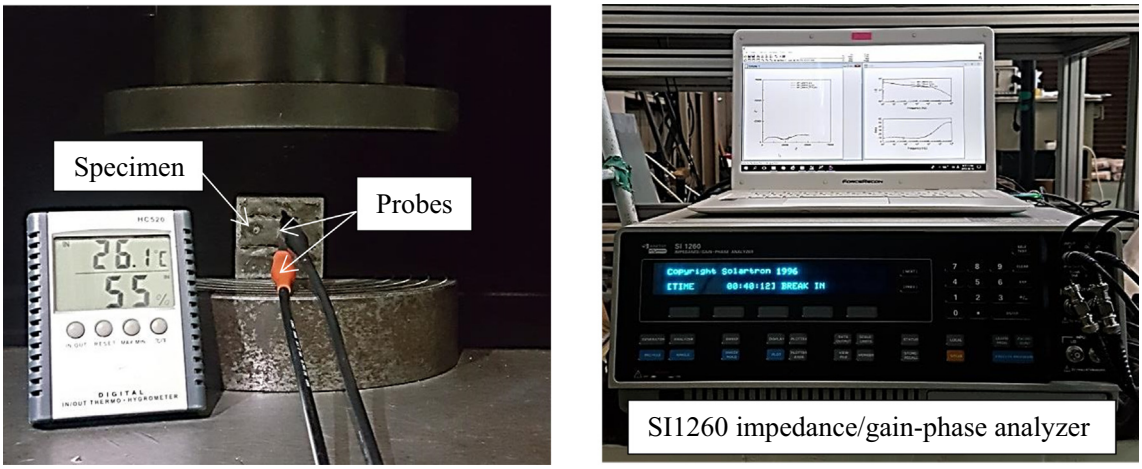

Fig. 4. Test set-up for AC electrical resistivity measurement.

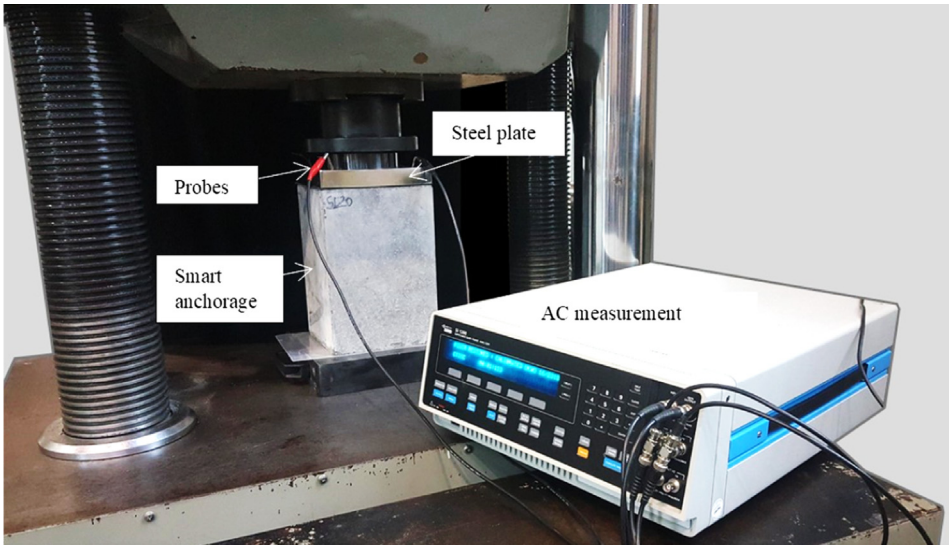

Fig. 5. Test set-up for the electrical resistivity measurement.

response of the specimens at each controlled compressive stress. The UTM under displacement control with a velocity of 1.0 mm/min was applied to the smart concrete anchorage specimens to measure the electromechanical response of the smart concrete anchorage. A steel plate with dimensions of 200 mm × 200 mm was placed on top of the smart concrete anchorage specimen. The AC measurement technique with a fixed frequency of 100 Hz was applied to measure the history of the electrical resistivity response during the tests. The fixed frequency value was determined from the frequency value at the cusp in the Nyquist plot.

To investigate the effects of temperature and humidity on the measured electrical impedance spectroscopy response, a chamber with controlled temperature and humidity was used to store the MSF specimens containing FSSAs and steel fibers. The MSF specimens were stored in the chamber for 1 day prior to measuring AC impedance. In this study, all the MSF specimens had already cured in hot water tank (90 °C) for 3 days and then stored 1 day in a laboratory at the temperature of 20 °C and humidity of 30% prior to keeping them in the chamber. Thus, the effects of a different temperature and ageing during short period of testing process (5 days) on the acceleration of the cement hydration of the specimens could be neglected since the hydration of the specimens was almost completed. Kang et al. [46] also reported that the strength of the UHPC specimens after heat treatment at high temperature (90 °C) did not increase between 7 and 28 days. The AC measurement technique with frequency ranging from 1 Hz to 10 MHz was used to measure the electrical resistivity of the cubic specimens under different temperature and humidity conditions.

4. Results and discussion

4.1. Comparative electrical responses

The electrical resistivity of the MSF, which contained both FSSAs and steel fibers, was clearly lower than those of the MS (containing FSSAs only) and MF (containing steel fibers only), but slightly higher than that of MFMW (containing both MWCNTs and steel fibers). The MSF exhibited the highest self-stress sensing capacity under compression among the studied smart concretes.

Fig. 6a shows the Nyquist plots for the different smart concretes (MF, MS, MSF, and MFMW). Fig. 6b shows the initial resistivity of the smart concretes, determined from the real impedance at the cusp of the Nyquist plots. As shown in Fig. 6b, the electrical resistivities of MSF, MS, and MF are 420, 500, and 1400 kΩ·cm, respectively. The electrical resistivity of MSF and/or the MS was clearly lower than that of the MF owing to uniform distribution of the FSSAs on the conductive networks. The MSL with a combination of the FSSAs and steel fibers produced a slightly lower electrical resistivity than the MS did. However, the electrical resistivity of the MSF is slightly higher than that (390 kΩ·cm) of the MFMW. The fiber shape of the MWCNTs helped produce a better conductive network than the use of particle powder [47]. In addition, the field emission and tunneling conduction from the nano-scale tip of the CNTs can significantly increase the conductivity of the composite containing MWCNTs [11]. The higher amount of superplasticizer (30% solid and 70% water) in the MFMW matrix can result in higher amount of free water as well as pore solution system, which can increase conductive network of the matrix.

Fig. 7 shows the impedance spectroscopy responses (using the Nyquist plot) of the smart concretes (MF, MS, MSF, and MFMW) under compressive stresses of 20, 40, 60, 80, and 100 MPa. Both the real and imaginary impedances of the smart concretes clearly decrease with the increase in the compressive stress. The electrical resistivity at the cusps was determined at the different controlled compressive stresses.

Fig. 8 shows the electrical resistivity change ratio, ($100 \times \rho_x/\rho_{20}$, %), of the smart concretes with the increase in the compressive load from 20 to 100 MPa. ρ_{20} is the electrical resistivity of the composites under a compressive stress of 20 MPa, and ρ_x is the electrical resistivity of the composites under controlled compressive stress values (20, 40, 60, 80, or 100 MPa). The electrical resistivity of all the specimens clearly decreased with the increase in the compressive stress from 20 to 100 MPa. The percentage reduction in the electrical resistivity ($100 \times (\rho_{20} - \rho_x)/\rho_{20}$) was calculated. Table 4 lists the results. According to results of Jia et al. shown in [1], the electrical resistivity of a concrete using steel slag decreased until approximately 35 MPa and then maintained and increased owing to the generation of crack in the matrix. The high compressive strength of matrices in this study could improve the self-stress sensing ability of composites as the compressive strain capacity in the elastic region increased. With the increase in the compressive stress following to the increase in the compressive strain, the distance between the conductive fillers (steel fibers, MWCNT, FSSAs, and their combination) decreased, whereas the connection between the conductive fillers increased.

The reduction in the electrical resistivity of the MSF is clearly higher than those of the MF and MS specimens under the

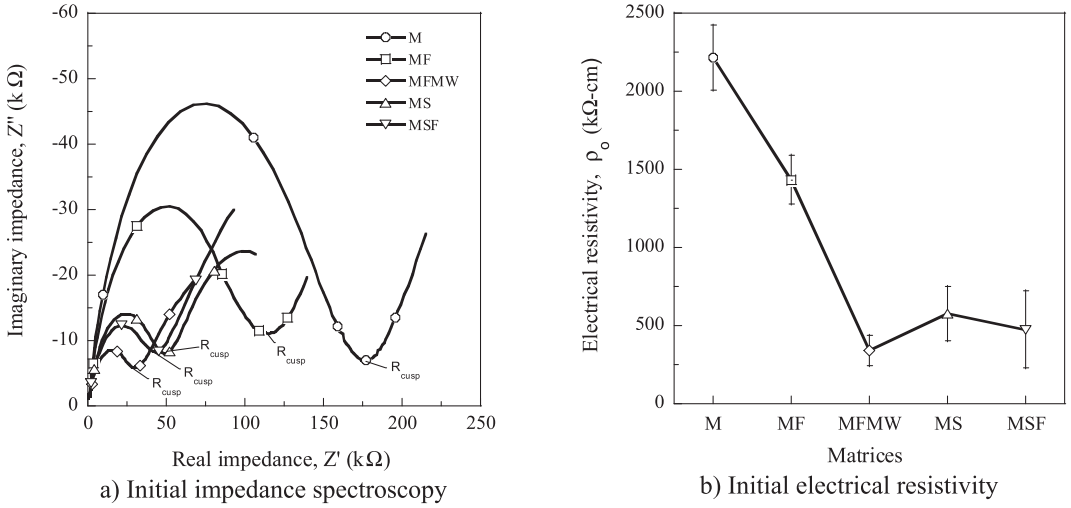

Fig. 6. The initial impedance spectroscopy and electrical resistivity of smart concretes.

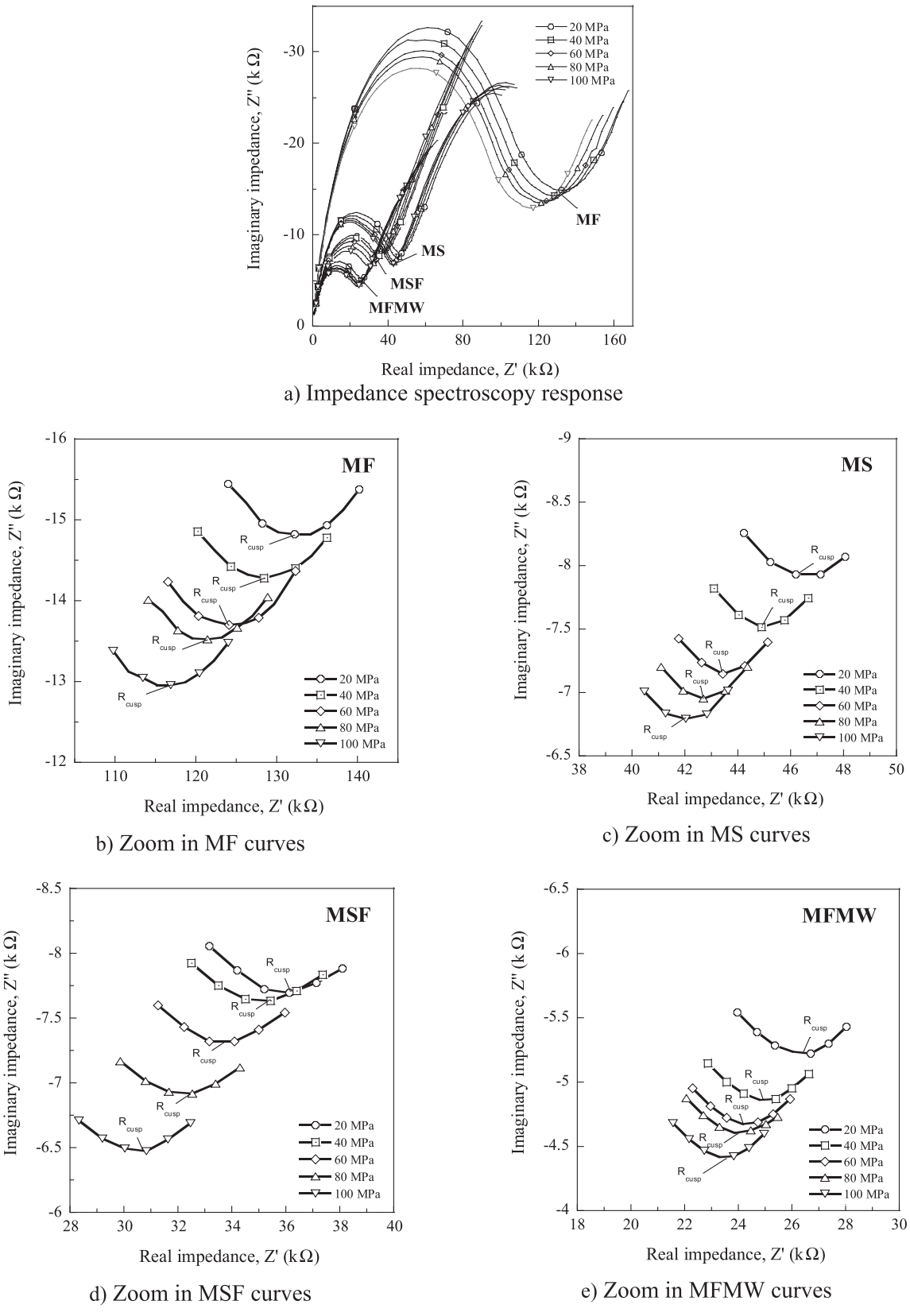

Fig. 7. The impedance spectroscopy responses of matrices under compressive stress.

controlled compressive stress values. With the increase in the compressive stress from 20 to 100 MPa, the electrical resistivities of the MSF, MF, and MS reduced by 15.65, 12.37, and 9.62%, respectively. The addition of steel fibers increased the connection between the conductive fillers including both steel fibers and FSSAs, whereas the use of the FSSAs, instead of silica sand, improved the piezoelec-

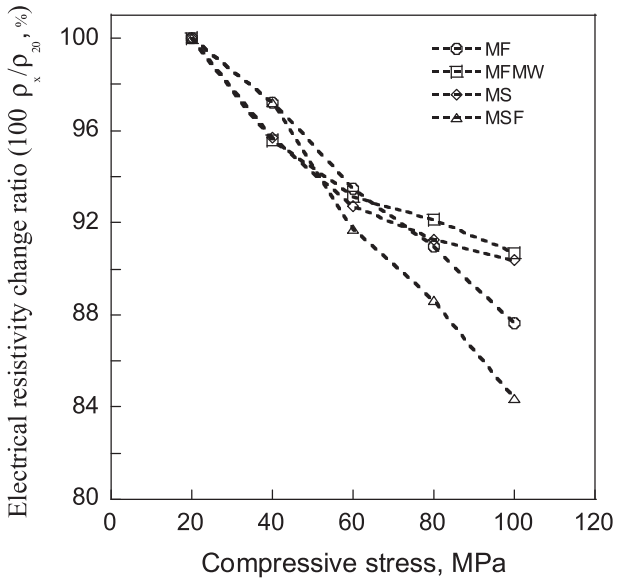

Fig. 8. The electrical resistivity response of smart concretes under compressive stress.

tric response owing to the quantum tunneling effect. The combination of FSSAs and steel fibers noticeably enhanced the conductive network as well as the sensitive piezoelectric response of the MSF. Fig. 9a captured the image of conductive fillers, including steel fibers and FSSAs, in the MSF matrix after compression. Fig. 9b shows a model of conductive network in the MSF composite while Fig. 9c and Fig. 9d show a conductive pathway in the composite prior to and under compressive loads, respectively. As the compressive stress/strain increased, the conductive network of the MSF composite enhanced owing to the contact of the conductive fillers. Moreover, as the conductive fillers including FSSAs and steel fibers came closer, the current passed through them owing to the quantum tunneling effect. The tunneling conduction is associated with the transmission conduction of electrons between disconnected yet close-enough fillers in concrete matrix [1,48–52]. Thus, as the compressive stress (strain) increased, the conductive pathway in the composites was enhanced and the electrical resistivity of composites consequently decreased. The content of conductive fillers including both FSSAs and steel fibers in the matrix could notably influence the conductive network as well as the self-stress sensing ability of the composite. Thus, effects of the content of FSSAs and steel fibers on the self-stress sensing should be further investigated in order to improve the self-stress sensing of the smart concrete.

The electrical resistivity of the MSF under compressive stress reduced to a greater extent compared to the MFMW. As listed in Table 4, the electrical resistivity of the MFMW at a compressive stress of 100 MPa reduced only by 9.30%, which is notably lower than that of the MSF. The greater reduction in the electrical resistivity of the MSF can be attributed to the well-structured conductive network owing to uniform distribution of FSSAs in the matrix (Fig. 9). However, the lower piezoelectric response of the MFMW could be due to the formation of significant initial conductive network pathways of the steel fibers and MWCNTs in the composite. In addition, the MSF (with a higher compressive strength, 184 MPa) generated lesser minor damages or fewer micro cracks inside than the MFMW (compressive strength of 154 MPa). Micro cracks can destroy the conductive network, consequently reducing the piezoelectric response of the composite [1]. Azhari and Banthia [53] also reported that smart concretes become less sensitive to load after micro crack generation. Thus, the self-stress sensing ability of the MSF with a higher strength was greater than that of the MFMW.

4.2. Self-stress sensing capacity of smart concrete anchorage made from MSF

Fig. 10 shows the history of the electrical resistivity response under compression (until 60 MPa) of the smart concrete anchorage made from the MSF. As shown in Fig. 10a, the three tested results provide a consistent correlation between the compressive stress and the fractional change in the resistivity, $FCR = (\rho_x - \rho_o)/\rho_o$, of the smart concrete anchorage. ρ_o is the initial electrical resistivity of the composites, and ρ_x is the electrical resistivity of the composites under a compressive stress. The electrical resistivity of the smart concrete anchorage specimens linearly decreased as the compressive stress increased from 0 to 60 MPa. The fractional change in the resistivity at a compressive stress of 60 MPa was −0.21. The negative value indicates a reduction in the electrical resistivity. As the compressive load was zero, i.e., when the specimen was unloaded, the electrical resistivity almost returned to the initial electrical resistivity value. It is clear that the linear piezoelectric response of the MSF matrix until 60 MPa of compressive stress in this study demonstrates a significantly improving self-stress sensing ability in comparison with current published reports (those until 20 MPa of compressive stress, as summarized in Table 1). It could be attributed to a high compressive strength of the MSF matrix in elastic region prior to matrix cracking and well-structured conductive network of FSSAs and steel fibers in the matrix. Under a compressive stress of 60 MPa, the specimens were expected to be within the linear elastic region without micro cracks because the compressive strength of the MSF was 184 MPa. As the compressive strain increased, the conductive fillers, including steel fibers and FSSAs, came closer, and consequently the electrical resistivity of the composite decreased almost linearly. The addition of both steel fibers and FSSAs helped increase the sensitive of the conductive network under compressive strain. Further, the addition of steel fibers helped increase the crack resistance, consequently improving the self-sensing ability of the smart concrete anchorage. As the compressive stress became zero

Table 4
Average reduction percentage in electrical resistivity under controlled compressive stress.

Compressive stress (MPa)	MF	MS	MSF	MFMW
The reduction percentage in electrical resistivity, 100. $(\rho_x - \rho_{20})/\rho_{20}$				
20	0	0	0	0
40	2.80 (1.42)	1.82 (1.45)	4.83 (3.29)	3.04 (2.40)
60	6.22 (1.69)	5.71 (1.20)	8.28 (2.98)	5.09 (3.24)
80	9.02 (2.4)	8.76 (1.25)	11.34 (3.51)	7.88 (4.65)
100	12.37 (2.53)	9.62 (1.41)	15.65 (1.99)	9.30 (5.69)

ρ_{20} and ρ_x are the electrical resistivity at 20 MPa in compressive strength and controlled stress value, respectively. The values in brackets are the standard deviation.

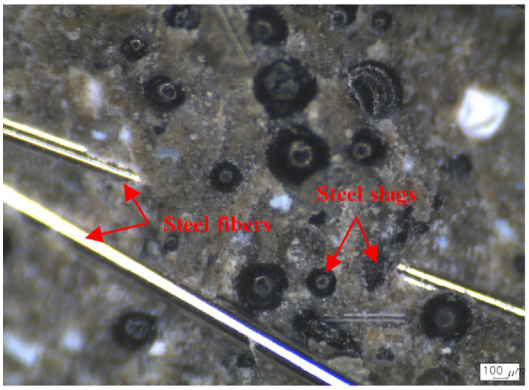

a) Image of conductive fillers in MSF matrix after compression

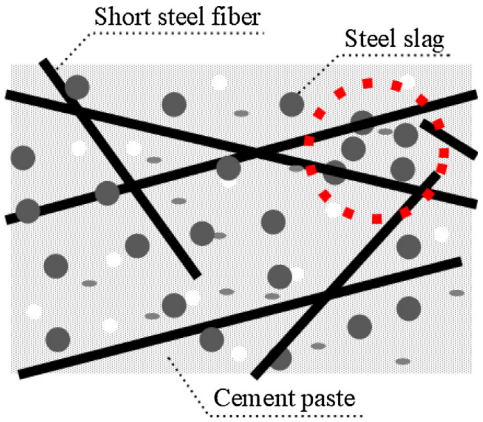

a) MSF matrix

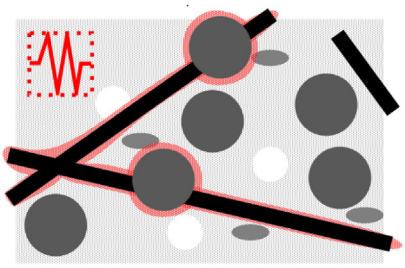

b) zoom in conductive pathway prior to loading

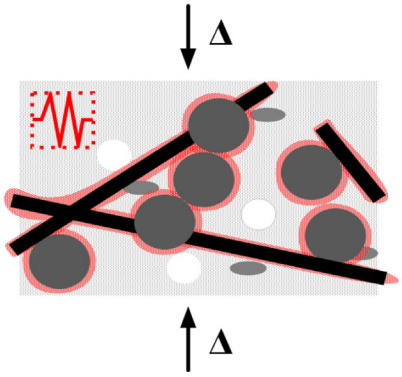

c) conductive pathway under compressive strain

Fig. 9. Conductive network of MSF matrix.

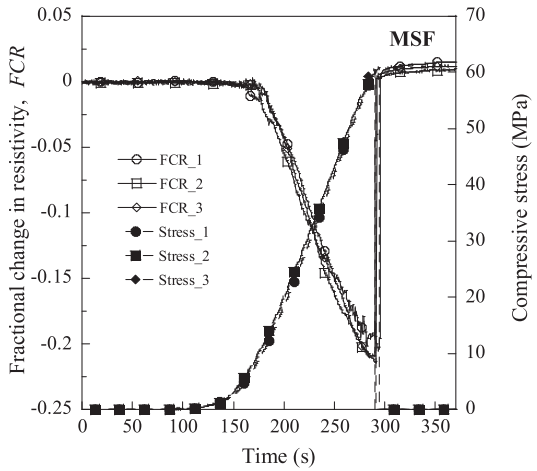

a) Tested results

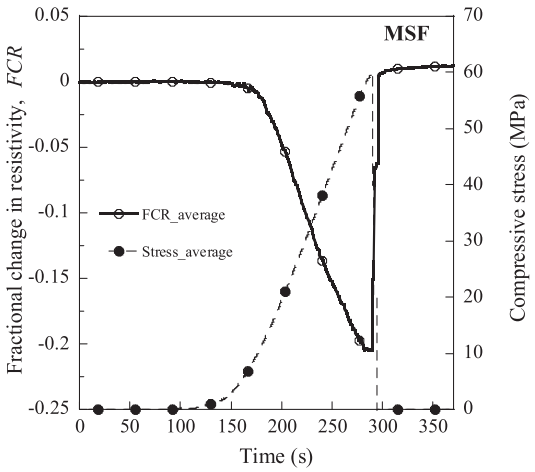

b) Average curve

Fig. 10. Electrical resistivity response of smart concrete anchorage using MSF under compression.

(unloading), the conductive fillers moved farther apart, and their connections decreased owing to the recovery of the strain of the specimens. The conductive network of the composite is restored after unloading. Thus, as the compressive stress decreased during the unloading process, the compressive strain of the specimens is fully recovered.

Fig. 11 shows the correlation between the fractional change in the resistivity, $FCR = (\rho_x - \rho_o)/\rho_o$, and the compressive stress. The fractional change in the resistivity linearly decreases with the increase in the compressive stress. Eq. (3) can be used to determine the compressive stress value (MPa) as a function of the *FCR* (negative value).

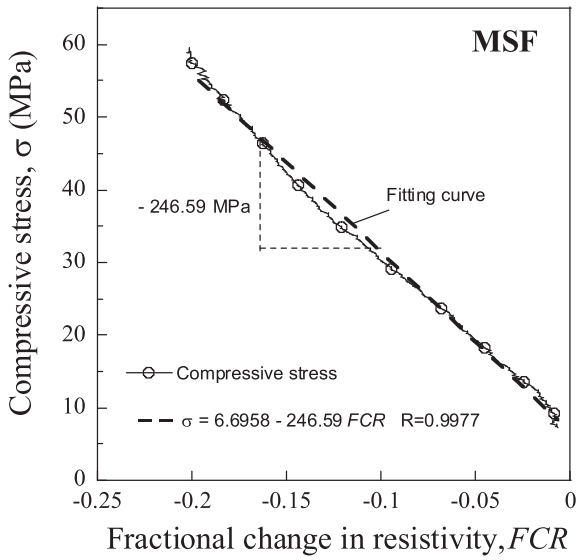

Fig. 11. The correlation between the electrical resistivity response and the compressive stress of the smart concrete anchorage using MSF.

$$\sigma = 6.6958 - 246.59FCR \quad (3)$$

The compressive stress of the smart concrete anchorage can be obtained by determining the fractional change in the resistivity. The stress gauge factor ($\Delta\sigma/\Delta FCR = -246.59$) can be utilized to monitor the change in the compressive stress of the smart concrete anchorage.

4.3. Effects of temperature and humidity on the electrical resistivity of MSF

The electrical resistivity of the MSF was sensitive to changes in the humidity and temperature. As the humidity and temperature increased, the electrical resistivity of the MSF decreased. However, the change in the electrical resistivity of the MSF corresponding to different humidity conditions was clearly lower compared to the conventional concrete (with a higher water-to-cement ratio) owing to the highly densified microstructure. Fig. 12 shows the effects of temperature and humidity on the electrical resistivity of the MSF.

As shown in Fig. 12a, the electrical resistivity of the MSF matrix is clearly influenced by the humidity. The electrical resistivity of the composite notably decreases from 700 to 300 kΩ·cm with the increase in the humidity from 30 to 100%. As the moisture increases, the amount of fluid in the pore solution system increases, and consequently, the mobility of the ions increases, i.e., the electrical current increases or the electrical resistivity decreases. Gjørv et al. [54] reported that the electrical resistivity of conventional concrete decreased from 600 to 7 kΩ·cm as the humidity increased from 20 to 100%. Larsen et al. [55] reported that the electrical resistivity of concrete increased six times as the moisture degree decreased from 88 to 66%. It is clear that the effect of humidity on the electrical resistivity of the MSF was notably lower compared to the concretes reported by Gjørv et al. [54] and Larsen et al. [55]. The lower change in the electrical resistivity under different humidity conditions might be due to the very high density of the MSF at a very low water-to-cement ratio (w/c = 0.2).

As shown in Fig. 12b, the temperature clearly influences the electrical resistivity of the MSF. With the increase in the temperature from 5 to 40 °C, the electrical resistivity of the composite significantly decreases from 1200 to 200 kΩ·cm at a humidity of 100%, whereas it decreases from 500 to 100 kΩ·cm at a humidity of 50%. Kim et al. [40] also reported the effect of temperature on the electrical resistivity of the UHPC matrix containing steel fibers (compressive strength of 180 MPa): the electrical resistivity of the UHPC decreased from 434.1 to 319.2 kΩ·cm as the temperature increased from 15 to 35°C at a controlled humidity of 60%. The temperature influences the behavior of the electrolyte solution in the pore solution system: as the temperature increases, the viscosity of the fluid in the pore system decreases, consequently increasing the mobility of the ions [56]. The effect of temperature on electrical resistivity of specimens at a high humidity (100%) was clearly higher than that at low humidity (50%). A greater humidity can provide greater free water in pore system, and consequently improve the movement of ion in pore solution system under influencing temperature, which results to increase the conductivity of the composite.

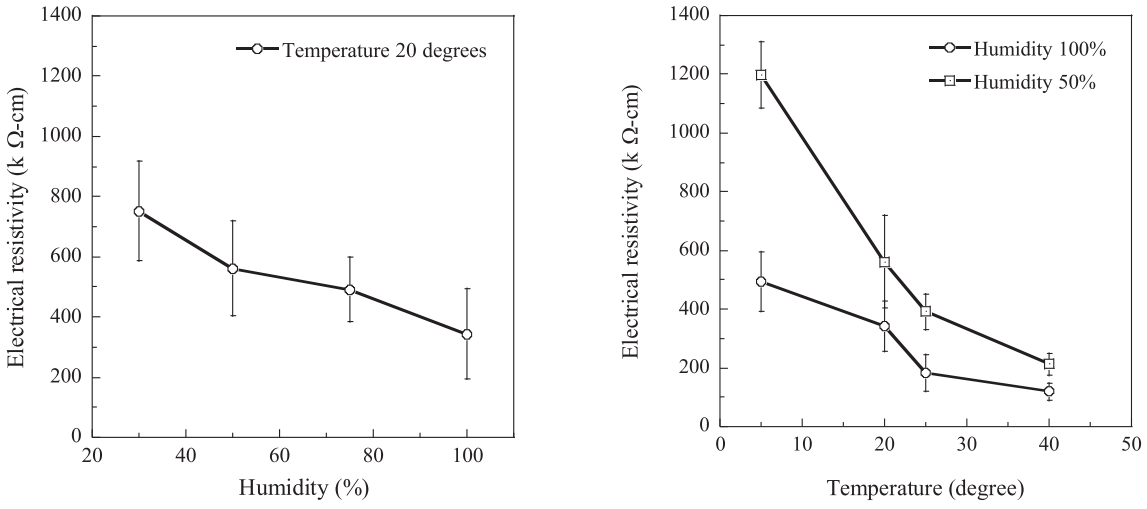

Fig. 12. Effect of the temperature and humidity on the electrical resistivity of MSF.

5. Conclusions

This experimental study investigated the self-stress sensing ability of a smart concrete (with a compressive strength of 184 MPa) containing FSSAs (ball shaped, with a maximum diameter of 0.39 mm) and steel fibers (with a length of 6 mm and a diameter of 0.2 mm) under compression using AC measurement with two probes. The piezoelectric response of a smart concrete containing FSSAs and steel fibers (MSF) was compared with that of smart concretes containing only steel fibers (MF), only FSSAs (MS), and both steel fibers and MWCNT (MFMW). The self-stress sensing ability of the MSF was utilized in a prestressing steel (PS) anchorage zone to monitor the loss of prestressing stress. In addition, the effects of temperature and humidity on the electrical resistivity of the smart concrete were investigated. The following conclusions can be drawn from this study:

- The smart concrete containing steel fibers and fine steel slag aggregates produced a clear reverse electrical resistivity response under compression. The electrical resistivity noticeably decreased with the increase in the compressive stress. The addition of short steel fibers helped significantly improved the conductive network, whereas the addition of FSSAs, instead of silica sand, helped enhance the piezoelectric sensitivity owing to the quantum tunneling effect.
- The smart concrete containing FSSAs and steel fibers exhibited a greater self-stress sensing ability than those containing only FSSAs or steel fibers or both MWCNTs and steel fibers.
- The self-stress sensing ability of the MSF under compression was utilized in the prestressing steel anchorage zone to monitor the loss of prestressing stress. A smart concrete anchorage made from MSF exhibited a linear piezoelectric response under compression until 60 MPa. The fractional change in the resistivity, $FCR = (\rho_x - \rho_o)/\rho_o$, of the smart concrete anchorage at a compressive stress of 60 MPa was −0.21.
- An equation, $\sigma = 6.6958 - 246.59FCR$, was derived, showing a linear correlation between the compressive stress (σ, until 60 MPa) and the fractional change in the resistivity of the smart concrete anchorage made from MSF. The compressive stress of the smart concrete anchorage could be analyzed by determining the fractional change in the resistivity. The stress gauge factor ($\Delta\sigma/\Delta FCR = -246.59$) could be used to monitor the change in the compressive stress of the smart concrete anchorage.
- The electrical resistivity of the MSF clearly decreased with the increase in the humidity and temperature. The change in the electrical resistivity of the MSF with varying humidity was clearly lower than that observed in conventional concrete owing to the highly densified microstructure.

Declaration of Competing Interest

None.

Acknowledgments

This research was supported by a grant (19CTAP-C143065-01) from the Infrastructure and Transportation Technology Promotion Research Program funded by the Ministry of Land, Infrastructure, and Transport of the Korean government. The opinions expressed in this paper are those of the authors and do not necessarily reflect the views of the sponsors.

References

[1] B. Han, X. Yu, J. Ou, in: Self-Sensing Concrete in Smart Structures, Butterworth Heinemann, Kidlington, 2014, https://doi.org/10.1016/C2013-0-14456-X.
[2] D.J. Kim, H.W. Noh, S.I. Choi, R.H. Hwang, S.Y. Lee, Smart concrete anchorage for monitoring pre-stressing loss, KoreaPatent. Submitted, 2019.
[3] S.C. Huang, W.W. Lin, M.T. Tsai, M.H. Chen, Fiber optic in-line distributed sensor for detection and localization of the pipeline leaks, Sens. Actuators, A Phys. 135 (2007) 570–579, https://doi.org/10.1016/j.sna.2006.10.010.
[4] Z. Chen, F. Ansari, Fiber optic acoustic emission distributed crack sensor for large structures, J. Struct. Control. 7 (2000) 119–129, https://doi.org/10.1002/stc.4300070108.
[5] M. Imai, M. Feng, Sensing optical fiber installation study for crack identification using a stimulated Brillouin-based strain sensor, Struct. Heal. Monit. 11 (2012) 501–509, https://doi.org/10.1177/1475921712442440.
[6] A. Billon, J.M. Henault, M. Quiertant, F. Taillade, A. Khadour, R.P. Martin, K. Benzarti, Qualification of a distributed optical fiber sensor bonded to the surface of a concrete structure: a methodology to obtain quantitative strain measurements, Smart Mater. Struct. 24 (2015) 1–13, https://doi.org/10.1088/0964-1726/24/11/115001.
[7] Z. Chen, S. Zhang, EM-based monitoring and probabilistic analysis of prestress loss of bonded tendons in PSC beams, Adv. Civ. Eng. 2018 (2018) 1–9.
[8] H. Abdel-Jaber, B. Glisic, Analysis of the status of pre-release cracks in prestressed concrete structures using long-gauge sensors, Smart Mater. Struct. 24 (2015) 1–12, https://doi.org/10.1088/0964-1726/24/2/025038.
[9] W. Hong, L. Kui, J. Yuchen, Y. Caiqian, W. Zhishen, H. Xiamin, Q. Qizhong, Self-sensing and quantitative assessment of prestressed concrete structures based on distributed long-gauge fiber Bragg grating sensors, J. Intell. Mater. Syst. Struct. 29 (2018) 1974–1985, https://doi.org/10.1177/1045389X18754355.
[10] B. Han, X. Yu, E. Kwon, A self-sensing carbon nanotube/cement composite for traffic monitoring, Nanotechnology 20 (2009) 1–5, https://doi.org/10.1088/0957-4484/20/44/445501.
[11] B. Han, K. Zhang, X. Yu, E. Kwon, J. Ou, Electrical characteristics and pressure-sensitive response measurements of carboxyl MWNT/cement composites, Cem. Concr. Compos. 34 (2012) 794–800, https://doi.org/10.1016/j.cemconcomp.2012.02.012.
[12] D.Y. Yoo, I. You, S.J. Lee, Electrical properties of cement-based composites with carbon nanotubes graphene, and graphite nanofibers, Sensors 17 (2017) 1–13, https://doi.org/10.3390/s17051064.
[13] B. Han, K. Zhang, X. Yu, E. Kwon, J. Ou, Nickel particle-based self-sensing pavement for vehicle detection, Meas. J. Int. Meas. Confed. 44 (2011) 1645–1650, https://doi.org/10.1016/j.measurement.2011.06.014.
[14] S. Wen, D.D.L. Chung, A comparative study of steel- and carbon-fiber cement as piezoresistive strain sensors, Adv. Cem. Res. 15 (2003) 119–128.
[15] D.D.L. Chung, Piezoresistive cement-based materials for strain sensing, J. Intell. Mater. Syst. Struct. 13 (2002) 599–609, https://doi.org/10.1106/104538902031861.
[16] Z.Q. Shi, D.D.L. Chung, Carbon fiber-reinforced concrete for traffic monitoring and weighing in motion, Cem. Concr. Res. 29 (1999) 435–439, https://doi.org/10.1016/S0008-8846(98)00204-X.
[17] X. Fu, W. Lu, D.D.L. Chung, Improving the strain-sensing ability of carbon fiber-reinforced cement by ozone treatment of the fibers, Cem. Concr. Res. 28 (1998) 183–187, https://doi.org/10.1016/S0008-8846(97)00265-2.
[18] D.M. Bontea, D.D.L. Chung, G.C. Lee, Damage in carbon fiber-reinforced concrete, monitored by electrical resistance measurement, Cem. Concr. Res. 30 (2000) 651–659, https://doi.org/10.1016/S0008-8846(00)00204-0.
[19] B. Han, J. Ou, Embedded piezoresistive cement-based stress/strain sensor, Sens. Actuators, A Phys. 138 (2007) 294–298, https://doi.org/10.1016/j.sna.2007.05.011.
[20] D.D.L. Chung, Self-monitoring structural materials, Mater. Sci. Eng. R Rep. 22 (1998) 57–78, https://doi.org/10.1016/S0927-796X(97)00021-1.
[21] A.O. Monteiro, P.B. Cachim, P.M.F.J. Costa, Electrical properties of cement-based composites containing carbon black particles, Mater. Today Proc. 2 (2015) 193–199, https://doi.org/10.1016/j.matpr.2015.04.021.
[22] M.S. Konsta-gdoutos, A.A. Chrysoula, Self sensing carbon nanotube (CNT) and nanofiber (CNF) cementitious composites for real time damage assessment in smart structures, Cem. Concr. Compos. 53 (2014) 162–169, https://doi.org/10.1016/j.cemconcomp.2014.07.003.
[23] B. Han, X. Yu, E. Kwon, J. Ou, Sensing properties of CNT-filled cement-based stress sensors, J. Civ. Struct Heal. Monit. 1 (2011) 17–24, https://doi.org/10.1007/s13349-010-0001-5.
[24] A. Al-Dahawi, O. Öztürk, F. Emami, G. Yildirim, M. Şahmaran, Effect of mixing methods on the electrical properties of cementitious composites incorporating different carbon-based materials, Constr. Build. Mater. 104 (2016) 160–168, https://doi.org/10.1016/j.conbuildmat.2015.12.072.
[25] Y. Wang, Y. Wang, B. Han, B. Wan, G. Cai, Z. Li, Strain monitoring of concrete components using embedded carbon nanofibers/epoxy sensors, Constr. Build. Mater. 186 (2018) 367–378, https://doi.org/10.1016/j.conbuildmat.2018.07.147.
[26] G. Yıldırım, M.H. Sarwary, A. Al-Dahawi, O. Öztürk, Ö. Anıl, M.S. Ahmaran, Piezoresistive behavior of CF- and CNT-based reinforced concrete beams subjected to static flexural loading: shear failure investigation, Constr. Build. Mater. 168 (2018) 266–279, https://doi.org/10.1016/j.conbuildmat.2018.02.124.

[27] Y. Ding, G. Liu, A. Hussain, F. Pacheco-torgal, Y. Zhang, Effect of steel fiber and carbon black on the self-sensing ability of concrete cracks under bending, Constr. Build. Mater. 207 (2019) 630–639, https://doi.org/10.1016/j.conbuildmat.2019.02.160.
[28] S. Ding, Y. Ruan, X. Yu, B. Han, Y. Ni, Self-monitoring of smart concrete column incorporating CNT/NCB composite fillers modified cementitious sensors, Constr. Build. Mater. 201 (2019) 127–137, https://doi.org/10.1016/j.conbuildmat.2018.12.203.
[29] I. You, D.Y. Yoo, S. Kim, M.J. Kim, G. Zi, Electrical and self-sensing properties of ultra-high-performance fiber-reinforced concrete with carbon nanotubes, Sensors (Switzerland) 17 (2017) 1–19, https://doi.org/10.3390/s17112481.
[30] S. Saxena, A.R. Tembhurkar, Impact of use of steel slag as coarse aggregate and wastewater on fresh and hardened properties of concrete, Constr. Build. Mater. 165 (2018) 126–137, https://doi.org/10.1016/j.conbuildmat.2018.01.030.
[31] H. Qasrawi, The use of steel slag aggregate to enhance the mechanical properties of recycled aggregate concrete and retain the environment, Constr. Build. Mater. 54 (2014) 298–304, https://doi.org/10.1016/j.conbuildmat.2013.12.063.
[32] Y. Jiang, T. Ling, C. Shi, S. Pan, Resources, conservation & recycling characteristics of steel slags and their use in cement and concrete — a review, Resour. Conserv. Recycl. 136 (2018) 187–197, https://doi.org/10.1016/j.resconrec.2018.04.023.
[33] T. Lu, Y. Chen, P. Shih, J. Chang, Use of basic oxygen furnace slag fines in the production of cementitious mortars and the effects on mortar expansion, Constr. Build. Mater. 167 (2018) 768–774, https://doi.org/10.1016/j.conbuildmat.2018.02.102.
[34] L. Rondi, G. Bregoli, S. Sorlini, L. Cominoli, C. Collivignarelli, G. Plizzari, Concrete with EAF steel slag as aggregate: a comprehensive technical and environmental characterisation, Compos. Part B 90 (2016) 195–202, https://doi.org/10.1016/j.compositesb.2015.12.022.
[35] I.L.H. Hansson, C.M. Hansson, Electrical resistivity measurements of Portland cement based materials, Cem. Concr. Res. 13 (1983) 675–683, https://doi.org/10.1016/0008-8846(83)90057-1.
[36] M. Sun, Z. Li, X. Song, Piezoelectric effect of hardened cement paste, Cem. Concr. Compos. 26 (2004) 717–720, https://doi.org/10.1016/S0958-9465(03)00104-5.
[37] S.J. Ford, J.D. Shane, T.O. Mason, Assignment of features in impedance spectra of the cement paste/steel system, Cem. Concr. Res. 28 (1998) 1737–1751.
[38] A. Peled, J.M. Torrents, T.O. Mason, S.P. Shah, E.J. Garboczi, Electrical impedance spectra to monitor damage during tensile loading of cement composites, ACI Mater. J. 98 (2001) 313–322, https://doi.org/10.14359/10400.
[39] H.V. Le, D.J. Kim, Effect of matrix cracking on electrical resistivity of high performance fiber reinforced cementitious composites in tension, Constr. Build. Mater. 156 (2017) 750–760, https://doi.org/10.1016/j.conbuildmat.2017.09.046.
[40] M.K. Kim, D.J. Kim, Y.K. An, Electro-mechanical self-sensing response of ultra-high-performance fiber-reinforced concrete in tension, Compos. Part B Eng. 134 (2018) 254–264, https://doi.org/10.1016/j.compositesb.2017.09.061.
[41] D.L. Nguyen, J. Song, C. Manathamsombat, D.J. Kim, Comparative electromechanical damage-sensing behaviors of six strain-hardening steel fiber-reinforced cementitious composites under direct tension, Compos. Part B Eng. 69 (2014) 159–168, https://doi.org/10.1016/j.compositesb.2014.09.037.
[42] J. Song, D.L. Nguyen, C. Manathamsombat, D.J. Kim, Effect of fiber volume content on electromechanical behavior of strain-hardening steel-fiber-reinforced cementitious composites, J. Compos. Mater. 49 (2015) 3621–3634, https://doi.org/10.1177/0021998314568169.
[43] W.J. McCarter, R. Brousseau, The A.C. response of hardened cement paste, Cem. Concr. Res. 20 (1990) 891–900.
[44] J.M. Torrents, T.O. Mason, E.J. Garboczi, Impedance spectra of fiber-reinforced cement-based composites: a modeling approach, Cem. Concr. Res. 30 (2000) 585–592, https://doi.org/10.1016/S0008-8846(00)00211-8.
[45] C.G. Berrocal, K. Hornbostel, M.R. Geiker, L. Ingemar, K. Lundgren, D.G. Bekas, Electrical resistivity measurements in steel fibre reinforced cementitious materials, Cem. Concr. Compos. 89 (2018) 216–229, https://doi.org/10.1016/j.cemconcomp.2018.03.015.
[46] Nicolas Roussel, Understanding the Rheology of Concrete, Woodhead Publishing Limited, 2012.
[47] S.H. Hwang, Y.B. Park, H.Y. Kwan, D.S. Bang, in: Smart Materials and Structures Based on Carbon Nanotube Composites, Intech Open, 2018, pp. 371–396, https://doi.org/10.5772/32009.
[48] W.S. Bao, S.A. Meguid, Z.H. Zhu, G.J. Weng, Tunneling resistance and its effect on the electrical conductivity of carbon nanotube nanocomposites, J. Appl. Phys. 111 (2013) 0937261–0937267, https://doi.org/10.1063/1.4716010.
[49] A.B. Oskouyi, U. Sundararaj, P. Mertiny, Tunneling conductivity and piezoresistivity of composites containing randomly dispersed conductive nano-platelets, Materials (Basel) 7 (2014) 2501–2521, https://doi.org/10.3390/ma7042501.
[50] E. García-Macías, A.D. Alessandro, R. Castro-Triguero, D. Pérez-Mira, F. Ubertini, Micromechanics modeling of the uniaxial strain-sensing property of carbon nanotube cement-matrix composites for SHM applications, Compos. Struct. 163 (2017) 195–215, https://doi.org/10.1016/j.compstruct.2016.12.014.
[51] J. Xu, W. Zhong, W. Yao, Modeling of conductivity in carbon fiber-reinforced cement-based composite, J. Mater. Sci. (2010) 3538–3546, https://doi.org/10.1007/s10853-010-4396-5.
[52] H. Li, H. Xiao, J. Ou, Effect of compressive strain on electrical resistivity of carbon black-filled cement-based composites, Cem. Concr. Compos. 28 (2006) 824–828, https://doi.org/10.1016/j.cemconcomp.2006.05.004.
[53] F. Azhari, N. Banthia, Cement-based sensors with carbon fibers and carbon nanotubes for piezoresistive sensing, Cem. Concr. Compos. 34 (2012) 866–873, https://doi.org/10.1016/j.cemconcomp.2012.04.007.
[54] O.E. Gjørv, Ø. Vennesland, El-Busaidy, in: Electrical Resistivity of Concrete in the Oceans, Offshore Technol Conf., 1977, pp. 581–589, https://doi.org/10.4043/2803-MS.
[55] C.K. Larsen, E.J. Sellevold, F. Askeland, J.M. Østvik, Ø. Vennesland, Electrical resistivity of concrete part II: influence of moisture content and temperature, in: Symp. Adv. Concr. through Sci. Eng., 2006, pp. 1–9.
[56] G. Monfore, The electrical resistivity of concrete, J. PCA Res. Dev. Lab. 10 (1968) 35–48.